Research Square

Preprints are preliminary reports that have not undergone peer review.
They should not be considered conclusive, used to inform clinical practice,
or referenced by the media as validated information.

Heavy precipitation and meteorological drought responses to solar irradiance reduction and stratospheric sulfate aerosol intervention

Yunfei Gao
Yellow River Basin Monitoring Center of Water-Soil Conservation and Eco-Environment
Liu Yang
yangliu.2017@outlook.com
Yellow River Basin Monitoring Center of Water-Soil Conservation and Eco-Environment
Dong Zhang
Yellow River Basin Monitoring Center of Water-Soil Conservation and Eco-Environment
Shanshan Zhou
Yellow River Basin Monitoring Center of Water-Soil Conservation and Eco-Environment
Jiaxin Zhang
Yellow River Basin Monitoring Center of Water-Soil Conservation and Eco-Environment
Xiang Jixiang
Xidian University

Article

Keywords: Solar radiation modification, Heavy precipitation, Consecutive dry days, Meteorological drought, GeoMIP

Posted Date: November 13th, 2026

DOI: https://doi.org/10.21203/rs.3.rs-11424352/v1

License: This work is licensed under a Creative Commons Attribution 4.0 International License.
Read Full License

Additional Declarations: No competing interests reported.

Heavy precipitation and meteorological drought responses to solar irradiance reduction and stratospheric sulfate aerosol intervention

Yunfei Gao[1, 2], Liu Yang[1, 3], Dong Zhang[1], Shanshan Zhou[1,4], Jiaxin Zhang[1,5], Xiang Jixiang[3]

[1] Yellow River Basin Monitoring Center of Water-Soil Conservation and Eco-Environment, 200 Fengcheng 3rd Road, Xi'an 710000, China

[2] Faculty of Geographical Science, Beijing Normal University, No.19 Xinjiekouwai Street, Haidian District, Beijing 100875, China

[3] Academy of Advanced Interdisciplinary Research, Xidian University, Xi'an, China

[4] College of Soil and Water Conservation, Northwest A&F University, Yangling 712100, China

[5] College of Hydrology and Water Resources, Hohai University,1 Xikang Road, Nanjing 210024, China

Corresponding author: Liu Yang;

Email Address of the Corresponding Author: yangliu.2017@outlook.com

Key Points:

IPSL simulations show weaker heavy precipitation under both G6 interventions.

G6sulfur yields more SPI-12 drought months than G6solar.

CDD and SPI-12 reveal different aspects of dry conditions.

Regional responses differ despite similar global surface temperatures.

Lower Rx5day can coincide spatially with more SPI-12 drought months.

Key words:

Solar radiation modification; Heavy precipitation; Consecutive dry days; Meteorological drought; GeoMIP

Abstract

Solar radiation modification can reduce warming, but heavy precipitation and meteorological drought may respond differently. Using one ensemble member of IPSL-CM6A-LR, we compare G6solar and G6sulfur with SSP5-8.5 over land north of 60°S during 2021–2100, focusing on 2081–2100. We assess annual maximum five-day precipitation (Rx5day), days with precipitation ≥10 mm (R10mm), consecutive dry days (CDD), and the fraction of months with a 12-month standardized precipitation index (SPI-12) ≤−1 relative to 1985–2014. Both interventions produce similar global mean surface temperatures but different land precipitation responses. During 2081–2100, land mean Rx5day decreases by 13.62 and 12.42 mm under G6solar and G6sulfur, respectively, while R10mm decreases by 3.13 and 4.15 days. The drought-month fraction increases by 0.60 and 4.03 percentage points; the 95% block bootstrap interval includes zero for G6solar but excludes zero for G6sulfur. East Asia shows lower Rx5day and more drought months, with small CDD changes. In western southern Africa, G6sulfur shortens CDD while increasing drought months. These single-model results show that weaker heavy precipitation and shorter dry spells do not necessarily indicate reduced accumulated precipitation deficits. Their assessment requires considering these distinct features of rainfall together.

1 Introduction

Climate warming is changing the amount, intensity, and timing of precipitation, with consequences for water availability, ecosystems, and human activities [1, 2, 3]. Observational analyses have detected anthropogenic influences on heavy precipitation and daily rainfall patterns, while climate projections indicate further increases in precipitation extremes under continued warming [4, 5, 6, 7]. Changes are not limited to the wettest events. Recent studies document amplified precipitation variability, examine the increasing contrast between wet and dry conditions, and show that rainfall frequency and intensity can affect vegetation in different ways [8, 9, 10]. The occurrence of damaging precipitation extremes in recent years further illustrates the need to understand changes beyond annual mean rainfall [11]. Even dry regions can experience increasing precipitation totals and stronger water-cycle activity, so a broad distinction between globally wetter and drier conditions can conceal important regional differences [12]. At the same time, drought can arise through different combinations of precipitation deficits, evaporative demand, and water storage changes, and projected drying

differs among precipitation, soil moisture, and runoff [13, 14]. These findings make it necessary to examine heavy precipitation and dry conditions together, while keeping their definitions and timescales distinct. A reduction in intense rainfall alone does not establish that a region has fewer dry months, and an increase in total rainfall does not describe how that rainfall is distributed through time.

Solar radiation modification (SRM) has been proposed as a means of cooling the climate by reflecting a small fraction of incoming sunlight or reducing incoming solar radiation. Stratospheric sulfate aerosol intervention is a widely studied approach, although it introduces risks and governance challenges and cannot remove the elevated greenhouse gas concentrations underlying climate change [15, 16, 17]. Within the CMIP6 and ScenarioMIP framework, the Geoengineering Model Intercomparison Project Phase 6 (GeoMIP6) provides coordinated experiments for assessing these responses [18, 19, 20]. G6solar reduces solar irradiance, whereas G6sulfur introduces stratospheric sulfate aerosols; both retain the SSP5-8.5 greenhouse gas background and aim to bring global mean temperature toward SSP2-4.5. Their shared temperature target does not imply an identical precipitation response. Moisture availability and atmospheric energy constraints influence precipitation differently, and the hydrological effects of solar forcing cannot be inferred from surface temperature alone [21, 22, 23]. Aerosol heating and circulation adjustments can also produce responses that idealized solar dimming does not reproduce [24, 25, 26]. G6 comparisons show uncertainty associated with aerosol distributions and model behavior, while process studies identify additional effects of sulfate absorption and stratospheric chemistry [27, 28, 29]. More recent GeoMIP experiment designs and initial results further show why intervention strategy and scenario must be considered when comparing outcomes [30, 31]. Reviews of hydrological outcomes likewise emphasize the importance of implementation strategy and regional conditions [32]. Consequently, similar cooling should be treated as a common background for evaluating hydrological differences, rather than as evidence that two interventions have equivalent effects on precipitation.

Research on climate intervention has increasingly moved from global mean temperature and precipitation toward regional extremes and dry conditions. Analysis of the Geoengineering Large Ensemble shows that stratospheric aerosol intervention can alter precipitation intensity, the occurrence of light and heavy rainfall, and the persistence of wet and dry spells [33]. Studies over China and Southeast Asia also show that reductions in projected heavy precipitation can

coexist with spatially uneven responses and changes in dry conditions [34, 35]. Assessments of the Muda River Basin, mainland Southeast Asia, and Hunan provide further evidence that the response depends on location, season, and the selected index [36, 37, 38]. Process-oriented studies help explain why regional differences are plausible: monsoon precipitation is sensitive to injection latitude and inter-hemispheric aerosol contrasts, while changes in atmospheric rivers provide another pathway through which intervention can redistribute precipitation [39, 40, 41]. A recent comparison over Afro-Asia likewise identifies spatial and temporal heterogeneity in the monsoon response to G6solar and G6sulfur [42]. Drought assessments add an important qualification. Liu et al. [43] show that changes in climatic water balance can differ among regions under G6sulfur, and Fu et al. [44] demonstrate opposing contributions from intervention-induced cooling and precipitation reductions to drought extremes. Together, these studies establish that SRM responses depend on the intervention, region, and metric. A complementary question is whether reduced heavy precipitation and reduced precipitation deficit occur at the same locations when both are evaluated using a consistent model, reference climate, and analysis period.

Addressing this question requires metrics that distinguish rainfall intensity, rainfall occurrence, dry-spell persistence, and accumulated precipitation deficit. Standardized daily indices and observational datasets provide a basis for evaluating these features, although climate models differ in their representation of extremes [45, 46, 47]. Here, annual maximum five-day precipitation (Rx5day) describes multiday rainfall intensity, the annual number of days with precipitation of at least 10 mm (R10mm) describes fixed-threshold rainfall occurrence, and consecutive dry days (CDD) describes the longest sequence of days below 1 mm within each calendar year. The standardized precipitation index (SPI) complements these measures by expressing accumulated precipitation relative to a reference distribution [48, 49]. Its interpretation depends on accumulation timescale and distribution fitting, whereas indices such as the standardized precipitation evapotranspiration index also include atmospheric evaporative demand [50, 51, 52]. A precipitation-only SPI assessment therefore answers a different question from a water-balance or soil-moisture drought assessment. Using SPI-12 alongside CDD can distinguish deficits in 12-month precipitation from the longest annual sequence of low-rainfall days. Their changes need not have the same sign. It is also important to distinguish the area showing a given direction of change from the area where the available record provides statistical

evidence for that change, because internal variability can obscure local precipitation responses [53]. Combining these metrics with area weighting, regional summaries, and spatial significance tests can clarify what is shared across indicators and what depends on their definitions.

Here, we use one ensemble member of IPSL-CM6A-LR to compare the effects of G6solar and G6sulfur on heavy precipitation and dry conditions over global land north of 60°S [54]. We examine annual changes during 2021–2100 and mean contrasts during 2081–2100. SSP5-8.5 is the main reference, the direct G6sulfur–G6solar contrast identifies differences between intervention methods, and SSP2-4.5 provides an additional climate background comparison. Rx5day, R10mm, and year-bounded CDD are recalculated consistently from daily precipitation. SPI-12 drought months are defined by SPI-12 ≤ -1 using a fixed 1985–2014 reference distribution. We ask three questions: how do the interventions change land mean heavy precipitation and dry conditions; where do their spatial and regional responses differ; and where does lower Rx5day coincide with a higher fraction of SPI-12 drought months? We address these questions using area-weighted statistics, IPCC AR6 land regions [55], block bootstrap intervals, and grid cell tests with false discovery rate correction. This framework provides a consistent comparison of responses within one model. It does not establish agreement across models, fully characterize internal variability, or identify the occurrence probability of compound drought and heavy-rainfall events.

2 Data and methods

2.1 Model data and experiments

We use SSP5-8.5, SSP2-4.5, G6solar, and G6sulfur simulations from IPSL-CM6A-LR to examine how two solar radiation intervention methods affect heavy precipitation and dry conditions over global land. We analyze the r1i1p1f1 member for all experiments. G6solar reduces solar irradiance, whereas G6sulfur uses stratospheric sulfate aerosols. Both intervention experiments retain the SSP5-8.5 greenhouse gas background and are designed to bring global mean temperature toward the SSP2-4.5 pathway.SSP5-8.5 is the main reference experiment. We calculate G6solar minus SSP5-8.5, G6sulfur minus SSP5-8.5, and G6sulfur minus G6solar. These contrasts describe changes relative to the high-emissions background and differences between the two interventions. SSP2-4.5 is used only for the climate background comparison in Figure 1. The variables include daily precipitation, monthly mean precipitation, and monthly

mean surface temperature. Daily precipitation for 2020–2100 is used to recalculate precipitation indices and future monthly precipitation totals. We examine the evolution over 2021–2100 and mean differences over 2081–2100. Precipitation in 2020 supplies the preceding months needed for SPI accumulation windows and is excluded from the reported analysis periods. All precipitation indices are calculated on the native grid, with 143 latitude points and 144 longitude points.

The main land domain includes land grid points at or north of 60°S. We identify land using the 1° land–sea classification mask supplied with NCL, retaining classes 1 and 3 for land and small islands. Each model grid point is assigned the category of the mask cell containing it; categorical values are not interpolated continuously. The latitude cutoff excludes the main Antarctic landmass but is not an exact continental boundary mask. Statistics including land south of 60°S provide a domain sensitivity check. For each metric, we retain a fixed set of grid cells with complete values in all three main experiments throughout 2021–2100. This prevents the averaging domain from changing between years or experiments. Rx5day, R10mm, and CDD cover 100% of the defined land area. Valid SPI-12 and SPI-3 cover 99.42% and 86.75%, respectively. Missing SPI values are not treated as months without drought. Individual metric statistics use that metric's valid land area as their denominator. Cross-metric domain checks and the classification in Figure 7 use the land common to all four main metrics, covering 99.42% of the study land domain.

Regional statistics use the IPCC AR6 land regions, intersected with the same land and validity masks. Figure 6 shows 12 regions distributed across the Americas, Africa, Eurasia, and Australia: WNA, CNA, NES, MED, WAF, CAF, WSAF, WCA, SAS, EAS, SEA, and NAU. Regional values are area weighted. Statistics for the complete set of available regions complement these selected examples, so interpretation does not rely only on global means or individual map features. Grid cells were assigned to the IPCC AR6 land regions according to the locations of their centers using regionmask version 0.12.0.

2.2 Heavy precipitation and consecutive dry days

We calculate Rx5day, R10mm, and CDD consistently from daily precipitation (Table 1). Before calculation, we check model, experiment, and member metadata, date completeness, duplicate dates, and the 24-hour time interval. Precipitation is expressed in mm day^{-1}. Original

fluxes in kg m^{-2} s^{-1} are multiplied by 86400, whereas previously converted daily precipitation is not converted again. Rx5day is the maximum precipitation accumulated over five consecutive days within each year, in mm. It describes the intensity of precipitation accumulated over several days. We calculate all five-day sums lying entirely within a calendar year and retain the largest. Windows crossing 31 December are therefore excluded from the annual Rx5day used here. R10mm is the annual number of days with precipitation of at least 10 mm, in days. It describes the frequency of precipitation exceeding a fixed threshold, whose degree of extremeness can differ among climate regions.

CDD is the longest annual sequence of days with precipitation below 1 mm day^{-1}, in days. The count is reset on 1 January, so dry spells crossing a year boundary are split. CDD therefore measures the longest dry spell within a calendar year rather than the full length of a spell extending across years. All three indices are calculated at each grid cell and year before area averaging. They are not calculated from the spatially averaged daily precipitation series.

2.3 Standardized precipitation index and drought month fraction

We calculate the standardized precipitation index, SPI, to complement the daily dry-spell information provided by CDD. SPI-12, based on 12-month accumulated precipitation, is the main drought metric. SPI-3 provides a supplementary comparison. SPI uses precipitation alone and describes meteorological drought relative to a fixed historical precipitation distribution. It does not include evaporative demand, soil moisture, or runoff and is not interpreted directly as agricultural or hydrological drought.The reference period is 1985–2014. Future monthly totals are obtained by summing daily precipitation for 2020–2100. Historical monthly precipitation was obtained from the IPSL-CM6A-LR historical simulation, member r1i1p1f1, covering 1850–2014. Monthly mean precipitation fluxes were converted to monthly totals by multiplying by 86400 and the number of days in each model-calendar month. Preceding months from 1984 were retained to calculate the 12-month accumulations ending in early 1985. The reference distribution was fitted using accumulations ending during 1985–2014.

At each grid cell, a historical reference distribution is fitted separately for each calendar month. Precipitation accumulated over k months ending in month t is calculated as:

$$X_t^{(k)} = \sum_{j=0}^{k-1} P_{t-j}\,, \qquad k = 3, 12$$

where Pt is monthly precipitation. For each ending calendar month, the 30 reference samples from 1985–2014 are used to fit a Gamma distribution to positive precipitation totals by maximum likelihood, with the location parameter fixed at zero. The cumulative probability accounting for zero precipitation is:

$$H_m(x) = q_m + (1 - q_m)G(x; \alpha_m, \beta_m),$$

$$q_m = \frac{n_{0,m}}{30}$$

SPI is then obtained through the inverse standard normal cumulative distribution:

$$\mathrm{SPI}_t^{(k)} = \Phi^{-1}\left[H_m\left(X_t^{(k)}\right)\right]$$

Here, m denotes the calendar month in which the accumulation window ends; α_m and β_m are the fitted Gamma shape and scale parameters; $n_{0,m}$ is the number of zero-precipitation samples; and Φ^{-1} is the inverse standard normal cumulative distribution function. The same historical parameters at each grid cell are applied to all future experiments.

A drought month is defined as a month with SPI-12 ≤ −1. The annual drought month fraction at grid cell i in year y is:

$$D_{i,y} = \frac{100}{12}\sum_{m=1}^{12} \mathbf{1}\,(\mathrm{SPI12}_{i,y,m} \le -1)$$

The regional mean drought month fraction over the analysis period and its difference between experiments are calculated as:

$$\bar{D}_R = \frac{1}{N_y}\sum_{y=1}^{N_y} \frac{\sum_{i\in R} A_i\, D_{i,y}}{\sum_{i\in R} A_i}$$

$$\Delta\overline{D}_R = \overline{D}_R^{a} - \overline{D}_R^{b}$$

Here, $1(\cdot)$ is an indicator function equal to 1 when the condition is satisfied and 0 otherwise; A_i is the area of a valid grid cell; N_y is the number of years, equal to 20 for 2081–2100; and a and b denote the experiments being compared. Drought month fractions are expressed as percentages, and differences are expressed in percentage points.

Fitting requires 30 complete, nonnegative reference samples for each calendar month, including at least 20 positive values with nonzero variance. Cumulative probabilities are clipped

to $[10^{-8}, 1-10^{-8}]$. Statistics use a fixed set of grid cells with valid parameters for all 12 calendar months and complete values in all three main experiments throughout 2021–2100. These validity criteria do not replace a distributional goodness-of-fit test.

2.4 Block bootstrap and multiple testing

Temporal sampling uncertainty is estimated using a circular moving-block bootstrap with five-year blocks and $B = 5000$ repetitions. The two experiments are resampled independently. For global land and regional annual series, the mean difference and its 95% bootstrap confidence interval are:

$$\Delta = \overline{X} - \overline{Y}$$

$$\Delta_b^* = \overline{X_b^*} - \overline{Y_b^*}$$

$$\mathrm{CI}_{95\%} = [Q_{0.025}(\Delta_b^*), Q_{0.975}(\Delta_b^*)]$$

where X and Y are annual series from the two experiments, the asterisk denotes a bootstrap sample, and Q_p denotes the $p-$quantile. Regional intervals are not adjusted for multiple comparisons.

For grid cell tests, each experiment's annual series is centered before resampling to construct the null distribution. Two-sided p values are calculated as:

$$X_t^0 = X_t - \bar{X},$$

$$Y_t^0 = Y_t - \bar{Y}$$

$$p = \frac{1 + \sum_{b=1}^{B} \mathbf{1}\left(\left|\Delta_b^{0*}\right| \geq \left|\hat{\Delta}\right|\right)}{B+1}$$

where Δ_b^{0*} is the resampled mean difference under the null hypothesis. The same temporal resampling indices are used across grid cells within each experiment. The *Benjamini–Hochberg* procedure controls the false discovery rate at $q = 0.05$, separately for each metric and contrast:

$$r = \max\left\{j : p_{(j)} \leq \frac{j}{M} q\right\}$$

where $p_{(j)}$ is the jth ordered p value and M is the number of tested grid cells. Cells with $p_i \leq p_{(r)}$ are hatched; no cells are selected if no rank satisfies the criterion.

SPI-12 tests use the 20 annual drought month fractions for 2081–2100, rather than treating 240 correlated months as independent samples. These estimates describe temporal sampling uncertainty in single-member simulations; short records and nonstationarity limit their interpretation, and model structural uncertainty is not included. (All analyses and figures were produced using Python 3.13.0, with NumPy 2.5.4, SciPy 1.18.1, pandas 3.0.6, xarray 2026.9.0, Matplotlib 3.11.2, Cartopy 0.26.0, regionmask 0.13.0, netCDF4 1.7.4, and cftime 1.6.6.)

3 Results

Figure 1 shows global mean surface temperature and land mean precipitation for the four experiments during 2021–2100. Surface temperature in both G6 experiments broadly follows SSP2-4.5, whereas SSP5-8.5 becomes substantially warmer toward the end of the century. During 2081–2100, global mean surface temperature is 19.94°C under SSP5-8.5 and approximately 17.60°C under both G6solar and G6sulfur. The reductions relative to SSP5-8.5 are about 2.33°C and 2.34°C, respectively. The corresponding SSP2-4.5 value is 17.58°C. The two interventions therefore produce similar cooling in their 20-year mean surface temperatures. Land precipitation does not approach SSP2-4.5 in the same way as temperature. During 2081–2100, land mean precipitation is 3.099 mm day^{-1} under SSP5-8.5, 2.981 mm day^{-1} under SSP2-4.5, 2.915 mm day^{-1} under G6solar, and 2.869 mm day^{-1} under G6sulfur. Relative to SSP5-8.5, the two interventions are lower by 0.184 and 0.229 mm day^{-1}. They are also lower than SSP2-4.5 by 0.066 and 0.112 mm day^{-1}. G6sulfur has approximately 0.045 mm day^{-1} less land precipitation than G6solar. Similar global mean surface temperatures can therefore accompany different land precipitation levels.

Figure 2 compares Rx5day, R10mm, CDD, and the SPI-12 drought month fraction over the same period. Mean Rx5day during 2021–2100 is 101.68 mm under SSP5-8.5, 94.85 mm under G6solar, and 96.22 mm under G6sulfur. Corresponding R10mm values are 30.22, 28.74, and 28.43 days. Both intervention experiments have lower mean multiday precipitation intensity and fewer days exceeding the fixed precipitation threshold than SSP5-8.5 over the full analysis period. The heavy precipitation differences are larger at the end of the century. During 2081–2100, Rx5day is 112.48 mm under SSP5-8.5, compared with 98.86 mm under G6solar and 100.06 mm under G6sulfur. The respective reductions are 13.62 and 12.42 mm, with 95% block bootstrap intervals of −15.80 to −11.52 mm and −14.44 to −10.69 mm. R10mm decreases from

32.42 days under SSP5-8.5 to 29.29 days under G6solar and 28.27 days under G6sulfur. These differences are −3.13 and −4.15 days, and both intervals exclude zero.

Differences between the interventions depend on the metric. G6sulfur has 1.02 fewer R10mm days than G6solar, with a 95% interval of −1.59 to −0.48 days. Its Rx5day is 1.20 mm higher, but the interval of −0.19 to 2.67 mm includes zero. The current record therefore supports fewer days reaching 10 mm under G6sulfur, while providing less clear evidence for a difference in global land mean Rx5day between the interventions. Global mean CDD changes are smaller. Late-century values are 69.40 days under SSP5-8.5, 67.03 days under G6solar, and 68.79 days under G6sulfur. G6solar is lower than SSP5-8.5 by 2.37 days, with an interval of −3.65 to −1.15 days. G6sulfur is lower by 0.61 days, but its interval of −2.11 to 0.93 days includes zero. G6sulfur exceeds G6solar by 1.75 days, with an interval of 0.49 to 3.03 days. Neither intervention shows a uniform increase in global land mean CDD relative to SSP5-8.5. SPI-12 describes a different aspect of precipitation deficit. The late-century area-weighted drought month fraction is 18.25% under SSP5-8.5, 18.86% under G6solar, and 22.29% under G6sulfur. The G6solar difference from SSP5-8.5 is 0.60 percentage points, with a 95% interval of −1.03 to 2.26 percentage points. The G6sulfur difference is 4.03 percentage points, with an interval of 1.60 to 6.36 percentage points. In the direct intervention comparison, G6sulfur is higher by 3.43 percentage points, with an interval of 1.26 to 5.57 percentage points.

Reduced heavy precipitation is therefore not accompanied by improvement in every dryness metric. Under G6sulfur in particular, lower land mean Rx5day and R10mm coexist with a higher SPI-12 drought month fraction. CDD measures the longest annual sequence of low-precipitation days, whereas SPI-12 measures how low 12-month precipitation is relative to the historical distribution. A small CDD response can therefore accompany an increased SPI-12 drought month fraction. An increased fraction does not establish that every drought event lasts longer.

Figure 3 shows negative Rx5day differences over most land in both interventions relative to SSP5-8.5. Larger negative values occur in Central Africa, South Asia, and parts of East and Southeast Asia. R10mm reductions are more spatially continuous, including the northern middle and high latitudes, Central Africa, parts of the Amazon region, and parts of Asia. Several of these areas pass the FDR adjustment. The maps agree with the lower global mean heavy precipitation indices, although localized increases remain. CDD has a more mixed spatial pattern. Shorter

CDD occurs around the Mediterranean and in parts of South America and southern Africa, whereas longer CDD occurs in parts of North Africa and the Eurasian interior. In the direct comparison, G6sulfur has longer CDD than G6solar in parts of North Africa, southern Africa, and Southeast Asia. Opposite signs can still occur within a region, so a local map feature cannot be assumed to describe the entire region.

The upper row of Figure 4 shows SPI-12 drought month fractions in the three experiments, and the lower row shows their differences. Relative to SSP5-8.5, both interventions reduce drought months around the Mediterranean and in parts of South America, while increasing them over northern Eurasia and several other areas. Positive differences under G6sulfur are more continuous over the Eurasian interior and are also prominent in parts of central and southern Africa. Significant increases and decreases both occur, showing that the global mean combines regional responses of opposite sign. The SPI-12 difference between G6sulfur and G6solar also has a regional pattern. G6sulfur has more drought months in parts of West Africa, central and southern Africa, Southeast Asia, and Eurasia, and fewer in parts of Australia. These are differences in long-term fractions relative to the other intervention. They do not describe a uniform local response, and darker colors alone do not establish statistical significance.

Figure 5 summarizes the area-weighted increases, decreases, and test outcomes. Decreases dominate Rx5day and R10mm, whereas increases and decreases occupy more similar areas for CDD. SPI-12 drought month fractions increase over a larger share of land. To compare metrics with exactly the same denominator, we also calculate fractions on the common valid domain, which covers 99.42% of the study land area. The precise area percentages below use this common domain, matching the denominator in Figure 7. On this common domain, Rx5day decreases over 78.33% of land under G6solar and 78.66% under G6sulfur relative to SSP5-8.5. FDR-significant decreases occupy 22.03% and 25.77% of the common valid land area. R10mm decreases over 76.23% and 78.88%, with significant decreases over 46.04% and 54.97%. A large area with negative differences does not mean that every negative cell passes the test. This distinction is especially evident for Rx5day.

CDD decreases over 56.71% and increases over 42.88% of common valid land under G6solar. Under G6sulfur, it decreases over 48.75% and increases over 50.84%. Significant decreases and increases under G6sulfur occupy 8.39% and 8.77%, respectively. Its small global

mean difference therefore partly reflects cancellation between opposite regional responses rather than an absence of changes everywhere. SPI-12 drought month fractions increase over 57.06% of common valid land under G6solar and 62.71% under G6sulfur. Significant increases occupy 9.78% and 17.99%, while significant decreases occupy 5.41% and 6.19%. G6sulfur therefore has both a larger area of increasing drought month fractions and a larger area of increases passing the test. This comparison of area fractions is descriptive; the difference between the two area percentages has not itself undergone a separate test.

Figure 6 examines regional mean differences and their 95% block bootstrap intervals. Regional responses do not always follow the global mean. All intervals discussed here describe temporal sampling without regional multiple-comparison adjustment. They help compare response magnitudes with variability in the current record but should not be interpreted as a jointly corrected set of regional findings.

The Mediterranean region, MED, has both shorter dry spells and fewer SPI-12 drought months under the interventions. Relative to SSP5-8.5, CDD decreases by 18.67 days under G6solar and 10.86 days under G6sulfur. Drought month fractions decrease by 22.88 and 15.51 percentage points. All four intervals exclude zero. R10mm, meanwhile, increases by 2.57 and 1.34 days. These responses differ from the global land decrease in R10mm and the global increase in drought month fraction under G6sulfur. Intervention responses are therefore not uniform across regions.

Central Africa, CAF, combines lower heavy precipitation indices with increased dryness metrics under G6sulfur. Rx5day decreases by 27.14 mm under G6solar and 19.27 mm under G6sulfur; R10mm decreases by 11.41 and 13.56 days. Under G6solar, the CDD difference is −0.07 days and the SPI-12 drought month fraction difference is 0.96 percentage points, with both intervals including zero. Under G6sulfur, CDD increases by 3.69 days and drought month fraction by 6.68 percentage points, with both intervals excluding zero. The interventions can therefore reduce heavy precipitation in the same region while producing different dryness responses.

West Southern Africa, WSAF, also shows a clear intervention contrast. Rx5day decreases by 12.25 mm under G6solar and 15.39 mm under G6sulfur, and CDD decreases by 12.34 and 4.85 days. However, the SPI-12 drought month fraction increases by 12.51 percentage points under

G6sulfur. The G6solar difference is −1.40 percentage points, with an interval including zero. In the direct comparison, G6sulfur exceeds G6solar by 13.91 percentage points, with an interval of 6.14 to 21.84 percentage points. Shorter CDD and more SPI-12 drought months occur together here, illustrating why the two dryness metrics cannot substitute for each other.

South Asia, SAS, and East Asia, EAS, show lower heavy precipitation indices and more SPI-12 drought months under both interventions. In South Asia, Rx5day decreases by 39.45 mm under G6solar and 27.64 mm under G6sulfur, while drought month fractions increase by 9.40 and 5.80 percentage points. In East Asia, Rx5day decreases by 14.73 and 12.83 mm, while drought month fractions increase by 5.18 and 5.81 percentage points. The regional intervals for these differences exclude zero. East Asian CDD differences are small and their intervals include zero, so its SPI-12 drying signal should not be summarized as a clear lengthening of the longest annual dry spell.

In Southeast Asia, SEA, the interventions differ mainly in precipitation day counts and dryness metrics. R10mm decreases by 3.36 days under G6solar and 10.95 days under G6sulfur. G6sulfur increases CDD by 4.11 days and SPI-12 drought month fraction by 4.06 percentage points relative to SSP5-8.5. Relative to G6solar, the increases are 6.70 days and 7.36 percentage points, and both intervals exclude zero. The direct Rx5day difference is 2.32 mm with an interval including zero, providing less clear evidence for an intervention difference in that metric.

Other regions show why uncertainty must remain part of the interpretation. Many intervals in Western North America, WNA, and Central North America, CNA, include zero, so point estimates alone do not establish a clear response direction. Northeastern South America, NES, has shorter CDD under both interventions, but its regional SPI-12 drought month fraction intervals include zero. Northern Australia, NAU, has Rx5day reductions of 15.75 and 14.38 mm with intervals excluding zero, whereas its CDD and drought month fraction intervals are wide. In West Africa, WAF, the SPI-12 drought month fraction under G6sulfur exceeds G6solar by 8.58 percentage points, with an interval of 3.34 to 13.64 percentage points. Differences between interventions are concentrated in particular regions and metrics; they do not support a claim that G6sulfur produces a stronger response everywhere or for every metric.

Figure 7 combines Rx5day and SPI-12 drought month fraction changes at the same grid cells to examine whether weaker heavy precipitation accompanies fewer drought months. Relative to

SSP5-8.5, lower Rx5day with more drought months is the largest class under both interventions. It occupies 49.51% of common valid land under G6solar and 55.50% under G6sulfur. This combination is widespread over northern Eurasia and parts of Africa and Asia. Lower multiday precipitation intensity can therefore occur in the same locations as more months with low accumulated precipitation relative to the historical reference. Decreases in both metrics occupy 20.07% of common valid land under G6solar and 15.89% under G6sulfur. Higher Rx5day with fewer drought months occupies 13.34% and 13.28%, while increases in both metrics occupy 7.55% and 7.21%. At least one metric is unchanged within the numerical tolerance over 9.53% and 8.12%, respectively. Both interventions thus contain several combinations of change. Lower global mean Rx5day alone does not establish improved precipitation-related conditions in every region.

The largest directional class is much larger than the part where both metrics pass their individual tests. Within the lower-Rx5day, more-drought-months class, cells passing both individual FDR-adjusted tests occupy only 3.72% of all common valid land under G6solar and 7.54% under G6sulfur. The larger fractions of 49.51% and 55.50% include cells not passing one or both tests. Hatching identifies the intersection of two individual test outcomes and should not be interpreted as a test of compound-event probability. In the direct G6sulfur minus G6solar comparison, lower Rx5day with more drought months occupies 35.75% of common valid land. Higher Rx5day with fewer drought months occupies 24.90%, increases in both metrics occupy 19.92%, and decreases in both occupy 13.67%. The direct intervention classification is more spatially fragmented than the comparisons with SSP5-8.5. This agrees with the preceding results: differences between interventions depend on both region and metric, and neither global surface temperature nor heavy precipitation alone summarizes the response of longer-term dry conditions.

4 Discussion

Why can weaker heavy precipitation, or even a shorter longest dry spell, coexist with more drought months? The regional results show that these responses can occur together. Relative to SSP5-8.5, East Asia exhibits lower Rx5day and a higher fraction of SPI-12 drought months, while its CDD response is comparatively small. In western southern Africa, G6sulfur shortens CDD but increases the fraction of SPI-12 drought months (Fig. 6). These results indicate that

heavy precipitation, dry-spell persistence, and accumulated precipitation deficit do not necessarily respond in the same direction. Consequently, weaker heavy precipitation or a shorter longest dry spell alone cannot establish whether precipitation-based drought has been alleviated.

Understanding this difference requires distinguishing how the indices summarize the precipitation record. Rx5day measures the largest five-day precipitation accumulation in each year, R10mm counts days reaching a fixed threshold, CDD describes the longest uninterrupted dry spell, and SPI-12 expresses 12-month accumulated precipitation relative to its historical distribution. These indices describe intensity, threshold exceedance, persistence, and accumulated deficit, respectively, and their changes need not be synchronized [47]. For example, fewer R10mm days can result from rainfall falling below 10 mm without a reduction in the number of wet days. Similarly, a weaker annual maximum five-day event does not determine whether precipitation during the remaining periods is sufficient. Heavy precipitation can contribute substantially to accumulated rainfall, but examining only the largest event cannot characterize the annual precipitation supply. The fraction of SPI-12 drought months instead depends on how often accumulated precipitation falls below a fixed historical threshold. Its response can involve changes in mean precipitation, variability, and the persistence of deficits.

East Asia particularly illustrates why a small change in the longest dry spell does not guarantee an unchanged accumulated precipitation deficit. Lower Rx5day occurs alongside a higher fraction of SPI-12 drought months, demonstrating that weaker precipitation maxima and more months with low accumulated precipitation can coexist at the regional scale. Even if the longest interval between wet days changes little, lower mean wet-day precipitation, changes in wet-day counts, or insufficient rainfall during the main wet season could make 12-month accumulations more likely to fall below the historical threshold. These explanations are compatible with the results, but their relative contributions cannot be determined from the four indices alone. Tye et al. [33] similarly found that changes in total precipitation and the longest dry spells were not consistently aligned in a large ensemble of stratospheric aerosol intervention simulations. The different index responses over East Asia therefore have a plausible interpretation in terms of precipitation statistics. However, this agreement does not attribute the response to a particular monsoon or circulation change.

Western southern Africa further illustrates that interrupting a dry spell and replenishing a precipitation deficit are different processes. In this region, G6sulfur produces shorter CDD but more SPI-12 drought months. By definition, a day with at least 1 mm of precipitation interrupts the CDD count, although this amount may provide little relief from a 12-month precipitation deficit. As a hypothetical example, inserting a single 1 mm day into the middle of a prolonged dry period can substantially shorten the longest dry spell while adding only 1 mm to accumulated precipitation. If precipitation on other wet days decreases, the accumulated total can nevertheless decline. This example shows how rainfall timing and amount can affect CDD and SPI-12 differently; it does not demonstrate that light rainfall has increased in the simulations analyzed here. Identifying the actual changes requires examining wet-day counts, mean wet-day precipitation, and monthly precipitation totals. These quantities would help establish whether shorter dry spells are accompanied by sufficient precipitation replenishment and identify the months in which deficits develop.

These findings indicate that assessments of solar radiation intervention should consider both short-duration heavy precipitation and precipitation supply over longer timescales. The spatial classification in Fig. 7 describes co-located changes in long-term statistics. It does not establish that weaker heavy precipitation causes additional drought months, nor does it quantify changes in the frequency of compound drought and heavy-precipitation events. Moreover, adjacent SPI-12 values share 11 months of precipitation, so a higher drought-month fraction can reflect more persistent deficits, more distinct episodes, or both. SPI probabilities also depend on the reference sample and fitted distribution [51]. Applying the same historical parameters maintains consistency across experiments but does not remove this uncertainty. The present analysis identifies changes in accumulated precipitation deficit relative to the historical precipitation climate; it cannot directly establish corresponding changes in soil moisture, runoff, or agricultural drought. Therefore, neither weaker heavy precipitation nor a shorter longest dry spell is sufficient evidence of an overall reduction in precipitation-related risks. Both need to be interpreted alongside changes in accumulated precipitation deficit.

5 Conclusions

This study shows that similar global mean cooling under G6solar and G6sulfur did not produce equivalent land precipitation responses. Although both interventions reduced land mean

Rx5day and R10mm relative to SSP5-8.5, these reductions did not consistently coincide with fewer SPI-12 drought months. The contrasting responses in East Asia and western southern Africa illustrate that accumulated precipitation deficits can increase without a substantial extension of the longest dry spell, and can even increase where that spell becomes shorter. The central implication is that weaker heavy precipitation and shorter dry spells cannot, on their own, establish relief from precipitation-based drought. Assessments of solar radiation intervention should therefore consider precipitation intensity, dry-spell persistence, and accumulated deficits together, rather than infer an overall improvement from a single indicator. These findings apply to the IPSL-CM6A-LR ensemble member examined here. Their robustness across models remains to be established, and the precipitation-based drought responses do not directly determine changes in soil moisture, runoff, or agricultural drought.

Funding Declaration

This work was supported by the Natural Science Basic Research Program of Shaanxi (Program No. 2026JC-YBQN-0349).

Author contributions

Yunfei Gao: conceptualization, software, formal analysis, visualization, and writing of the original draft. Liu Yang: conceptualization, methodology, supervision, and review and editing of the manuscript. Dong Zhang: data curation and validation. Shanshan Zhou: methodology and validation. Jiaxin Zhang: data curation and visualization. Xiang Jixiang: supervision and review and editing of the manuscript.

Data availability

The IPSL-CM6A-LR CMIP6 and GeoMIP simulations used in this study are distributed through the Earth System Grid Federation (ESGF). The data comprise historical monthly precipitation and daily precipitation, monthly precipitation, and monthly surface temperature for the experiments and periods specified in Methods, using member r1i1p1f1.

Competing interests

The authors declare no competing interests.

References

1. Allan, R. P., Willett, K. M., John, V. O. & Trent, T. Global Changes in Water Vapor 1979–2020. *J. Geophys. Res. Atmos.* **127,** e2022JD036728 (2022). https://doi.org/10.1029/2022jd036728

2. O'Gorman, P. A. Precipitation Extremes Under Climate Change. *Curr. Clim. Change Rep.* **1,** 49–59 (2015). https://doi.org/10.1007/s40641-015-0009-3

3. Seneviratne, S. I. et al. Weather and Climate Extreme Events in a Changing Climate. In *Climate Change 2021: The Physical Science Basis* (eds Masson-Delmotte, V. et al.) 1513–1766 (Cambridge University Press, 2021). https://doi.org/10.1017/9781009157896.013

4. Ham, Y.-G. et al. Anthropogenic fingerprints in daily precipitation revealed by deep learning. *Nature* **622,** 301–307 (2023). https://doi.org/10.1038/s41586-023-06474-x

5. Li, C. et al. Changes in Annual Extremes of Daily Temperature and Precipitation in CMIP6 Models. *J. Clim.* **34,** 3441–3460 (2021). https://doi.org/10.1175/jcli-d-19-1013.1

6. Madakumbura, G. D., Thackeray, C. W., Norris, J., Goldenson, N. & Hall, A. Anthropogenic influence on extreme precipitation over global land areas seen in multiple observational datasets. *Nat. Commun.* **12,** 3944 (2021). https://doi.org/10.1038/s41467-021-24262-x

7. Thackeray, C. W., Hall, A., Norris, J. & Chen, D. Constraining the increased frequency of global precipitation extremes under warming. *Nat. Clim. Chang.* **12,** 441–448 (2022). https://doi.org/10.1038/s41558-022-01329-1

8. Feldman, A. F. et al. Plant responses to changing rainfall frequency and intensity. *Nat. Rev. Earth Environ.* **5,** 276–294 (2024). https://doi.org/10.1038/s43017-024-00534-0

9. Swain, D. L. et al. Hydroclimate volatility on a warming Earth. *Nat. Rev. Earth Environ.* **6,** 35–50 (2025). https://doi.org/10.1038/s43017-024-00624-z

10. Zhang, W., Zhou, T. & Wu, P. Anthropogenic amplification of precipitation variability over the past century. *Science* **385,** 427–432 (2024). https://doi.org/10.1126/science.adp0212

11. Green, A. C., Fowler, H. J., Blenkinsop, S. & Davies, P. A. Precipitation extremes in 2024. *Nat. Rev. Earth Environ.* **6,** 243–245 (2025). https://doi.org/10.1038/s43017-025-00666-x

12. Guan, Y. et al. Human-induced intensification of terrestrial water cycle in dry regions of the globe. *npj Clim. Atmos. Sci.* **7,** 45 (2024). https://doi.org/10.1038/s41612-024-00590-9

13. Ault, T. R. On the essentials of drought in a changing climate. *Science* **368,** 256–260 (2020). https://doi.org/10.1126/science.aaz5492

14. Cook, B. I. et al. Twenty-First Century Drought Projections in the CMIP6 Forcing Scenarios. *Earth's Future* **8,** e2019EF001461 (2020). https://doi.org/10.1029/2019ef001461

15. Crutzen, P. J. Albedo Enhancement by Stratospheric Sulfur Injections: A Contribution to Resolve a Policy Dilemma?. *Climatic Change* **77,** 211–220 (2006). https://doi.org/10.1007/s10584-006-9101-y

16. National Academies of Sciences, Engineering, and Medicine. *Reflecting Sunlight: Recommendations for Solar Geoengineering Research and Research Governance* (The National Academies Press, 2021). https://doi.org/10.17226/25762

17. Parson, E. A. & Keith, D. W. Solar Geoengineering: History, Methods, Governance, Prospects. *Annu. Rev. Environ. Resour.* **49,** 337–366 (2024). https://doi.org/10.1146/annurev-environ-112321-081911

18. Eyring, V. et al. Overview of the Coupled Model Intercomparison Project Phase 6 (CMIP6) experimental design and organization. *Geosci. Model Dev.* **9,** 1937–1958 (2016). https://doi.org/10.5194/gmd-9-1937-2016

19. Kravitz, B. et al. The Geoengineering Model Intercomparison Project Phase 6 (GeoMIP6): simulation design and preliminary results. *Geosci. Model Dev.* **8,** 3379–3392 (2015). https://doi.org/10.5194/gmd-8-3379-2015

20. O'Neill, B. C. et al. The Scenario Model Intercomparison Project (ScenarioMIP) for CMIP6. *Geosci. Model Dev.* **9,** 3461–3482 (2016). https://doi.org/10.5194/gmd-9-3461-2016

21. Held, I. M. & Soden, B. J. Robust Responses of the Hydrological Cycle to Global Warming. *J. Clim.* **19,** 5686–5699 (2006). https://doi.org/10.1175/jcli3990.1

22. Pendergrass, A. G. & Hartmann, D. L. The Atmospheric Energy Constraint on Global-Mean Precipitation Change. *J. Clim.* **27,** 757–768 (2014). https://doi.org/10.1175/jcli-d-13-00163.1

23. Tilmes, S. et al. The hydrological impact of geoengineering in the Geoengineering Model Intercomparison Project (GeoMIP). *J. Geophys. Res. Atmos.* **118,** 11036–11058 (2013). https://doi.org/10.1002/jgrd.50868

24. Ferraro, A. J., Highwood, E. J. & Charlton-Perez, A. J. Weakened tropical circulation and reduced precipitation in response to geoengineering. *Environ. Res. Lett.* **9,** 014001 (2014). https://doi.org/10.1088/1748-9326/9/1/014001

25. Jones, A. et al. North Atlantic Oscillation response in GeoMIP experiments G6solar and G6sulfur: why detailed modelling is needed for understanding regional implications of solar radiation management. *Atmos. Chem. Phys.* **21,** 1287–1304 (2021). https://doi.org/10.5194/acp-21-1287-2021

26. Simpson, I. R. et al. The Regional Hydroclimate Response to Stratospheric Sulfate Geoengineering and the Role of Stratospheric Heating. *J. Geophys. Res. Atmos.* **124,** 12587–12616 (2019). https://doi.org/10.1029/2019jd031093

27. Tilmes, S. et al. Stratospheric ozone response to sulfate aerosol and solar dimming climate interventions based on the G6 Geoengineering Model Intercomparison Project (GeoMIP) simulations. *Atmos. Chem. Phys.* **22,** 4557–4579 (2022). https://doi.org/10.5194/acp-22-4557-2022

28. Visioni, D. et al. Identifying the sources of uncertainty in climate model simulations of solar radiation modification with the G6sulfur and G6solar Geoengineering Model Intercomparison Project (GeoMIP) simulations. *Atmos. Chem. Phys.* **21,** 10039–10063 (2021). https://doi.org/10.5194/acp-21-10039-2021

29. Wunderlin, E. et al. Side Effects of Sulfur-Based Geoengineering Due To Absorptivity of Sulfate Aerosols. *Geophys. Res. Lett.* **51,** e2023GL107285 (2024). https://doi.org/10.1029/2023gl107285

30. Lee, W. R. et al. G6-1.5K-SAI and G6sulfur: changes in impacts and uncertainty depending on stratospheric aerosol injection strategy in the Geoengineering Model Intercomparison Project. *Atmos. Chem. Phys.* **26,** 7463–7483 (2026). https://doi.org/10.5194/acp-26-7463-2026

31. Visioni, D. et al. G6-1.5K-SAI: a new Geoengineering Model Intercomparison Project (GeoMIP) experiment integrating recent advances in solar radiation modification studies. *Geosci. Model Dev.* **17,** 2583–2596 (2024). https://doi.org/10.5194/gmd-17-2583-2024

32. Ricke, K., Wan, J. S., Saenger, M. & Lutsko, N. J. Hydrological Consequences of Solar Geoengineering. *Annu. Rev. Earth Planet. Sci.* **51,** 447–470 (2023). https://doi.org/10.1146/annurev-earth-031920-083456

33. Tye, M. R. et al. Indices of extremes: geographic patterns of change in extremes and associated vegetation impacts under climate intervention. *Earth Syst. Dyn.* **13,** 1233–1257 (2022). https://doi.org/10.5194/esd-13-1233-2022

34. Feng, Z.-Q. et al. Effects of solar radiation modification on precipitation extremes in Southeast Asia: Insights from the GeoMIP G6 experiments. *Adv. Clim. Change Res.* **16,** 591–605 (2025). https://doi.org/10.1016/j.accre.2025.04.009

35. Wang, O. et al. Projected future changes in extreme precipitation over China under stratospheric aerosol intervention in the UKESM1 climate model. *Atmos. Chem. Phys.* **24,** 12355–12373 (2024). https://doi.org/10.5194/acp-24-12355-2024

36. Narenpitak, P., Kongkulsiri, S., Tomkratoke, S. & Sirisup, S. Regional impacts of solar radiation modification on surface temperature and precipitation in Mainland Southeast Asia and the adjacent oceans. *Sci. Rep.* **14,** 22713 (2024). https://doi.org/10.1038/s41598-024-73149-6

37. Tan, M. L. et al. Assessment of solar geoengineering impact on precipitation and temperature extremes in the Muda River Basin, Malaysia using CMIP6 SSP and GeoMIP6 G6 simulations. *Sci. Total Environ.* **948,** 174817 (2024). https://doi.org/10.1016/j.scitotenv.2024.174817

38. Tang, H., Tan, M. L., Feng, Z., Samat, N. & Zhang, F. Solar Radiation Modification impact on precipitation and temperature extremes in Hunan, China. *J. Hydrol. Reg. Stud.* **61,** 102728 (2025). https://doi.org/10.1016/j.ejrh.2025.102728

39. Krishnamohan, K. S. & Bala, G. Sensitivity of tropical monsoon precipitation to the latitude of stratospheric aerosol injections. *Clim. Dyn.* **59,** 151–168 (2022). https://doi.org/10.1007/s00382-021-06121-z

40. Liang, J. & Haywood, J. Future changes in atmospheric rivers over East Asia under stratospheric aerosol intervention. *Atmos. Chem. Phys.* **23,** 1687–1703 (2023). https://doi.org/10.5194/acp-23-1687-2023

41. Roose, S., Bala, G., Krishnamohan, K. S., Cao, L. & Caldeira, K. Quantification of tropical monsoon precipitation changes in terms of interhemispheric differences in stratospheric sulfate aerosol optical depth. *Clim. Dyn.* **61,** 4243–4258 (2023). https://doi.org/10.1007/s00382-023-06799-3

42. Adeliyi, T. E. & Akinsanola, A. A. Sensitivity of projected Afro-Asian monsoon precipitation to solar radiation management. *Sci. Total Environ.* **1024,** 181634 (2026). https://doi.org/10.1016/j.scitotenv.2026.181634

43. Liu, Z., Lang, X. & Jiang, D. Stratospheric Aerosol Injection Geoengineering Would Mitigate Greenhouse Gas-Induced Drying and Affect Global Drought Patterns. *J. Geophys. Res. Atmos.* **129,** e2023JD039988 (2024). https://doi.org/10.1029/2023jd039988

44. Fu, W., Yue, X., Tian, C., Xu, R. & Guo, Y. Unequal socioeconomic exposure to drought extremes induced by stratospheric aerosol injection. *Atmos. Chem. Phys.* **25,** 13103–13121 (2025). https://doi.org/10.5194/acp-25-13103-2025

45. Dunn, R. J. H. et al. Development of an Updated Global Land In Situ-Based Data Set of Temperature and Precipitation Extremes: HadEX3. *J. Geophys. Res. Atmos.* **125,** e2019JD032263 (2020). https://doi.org/10.1029/2019jd032263

46. Kim, Y.-H., Min, S.-K., Zhang, X., Sillmann, J. & Sandstad, M. Evaluation of the CMIP6 multi-model ensemble for climate extreme indices. *Weather Clim. Extrem.* **29,** 100269 (2020). https://doi.org/10.1016/j.wace.2020.100269

47. Zhang, X. et al. Indices for monitoring changes in extremes based on daily temperature and precipitation data. *WIREs Clim. Change* **2,** 851–870 (2011). https://doi.org/10.1002/wcc.147

48. Lloyd-Hughes, B. & Saunders, M. A. A drought climatology for Europe. *Int. J. Climatol.* **22,** 1571–1592 (2002). https://doi.org/10.1002/joc.846

49. World Meteorological Organization. *Standardized Precipitation Index User Guide* (WMO-No. 1090, World Meteorological Organization, 2012). https://digitalcommons.unl.edu/droughtfacpub/209/

50. Mukherjee, S., Mishra, A. & Trenberth, K. E. Climate Change and Drought: a Perspective on Drought Indices. *Curr. Clim. Change Rep.* **4,** 145–163 (2018). https://doi.org/10.1007/s40641-018-0098-x

51. Stagge, J. H., Tallaksen, L. M., Gudmundsson, L., Van Loon, A. F. & Stahl, K. Candidate Distributions for Climatological Drought Indices (SPI and SPEI). *Int. J. Climatol.* **35,** 4027–4040 (2015). https://doi.org/10.1002/joc.4267

52. Vicente-Serrano, S. M., Beguería, S. & López-Moreno, J. I. A Multiscalar Drought Index Sensitive to Global Warming: The Standardized Precipitation Evapotranspiration Index. *J. Clim.* **23,** 1696–1718 (2010). https://doi.org/10.1175/2009jcli2909.1

53. Li, C., Liu, J., Du, F., Zwiers, F. W. & Feng, G. Increasing certainty in projected local extreme precipitation change. *Nat. Commun.* **16,** 850 (2025). https://doi.org/10.1038/s41467-025-56235-9

54. Boucher, O. et al. Presentation and Evaluation of the IPSL-CM6A-LR Climate Model. *J. Adv. Model. Earth Syst.* **12,** e2019MS002010 (2020). https://doi.org/10.1029/2019ms002010

55. Iturbide, M. et al. An update of IPCC climate reference regions for subcontinental analysis of climate model data: definition and aggregated datasets. *Earth Syst. Sci. Data* **12,** 2959–2970 (2020). https://doi.org/10.5194/essd-12-2959-2020

56. Künsch, H. R. The jackknife and the bootstrap for general stationary observations. *Ann. Stat.* **17,** 1217–1241 (1989). https://doi.org/10.1214/aos/1176347265

57. Benjamini, Y. & Hochberg, Y. Controlling the false discovery rate: a practical and powerful approach to multiple testing. *J. R. Stat. Soc. B* **57,** 289–300 (1995). https://doi.org/10.1111/j.2517-6161.1995.tb02031.x

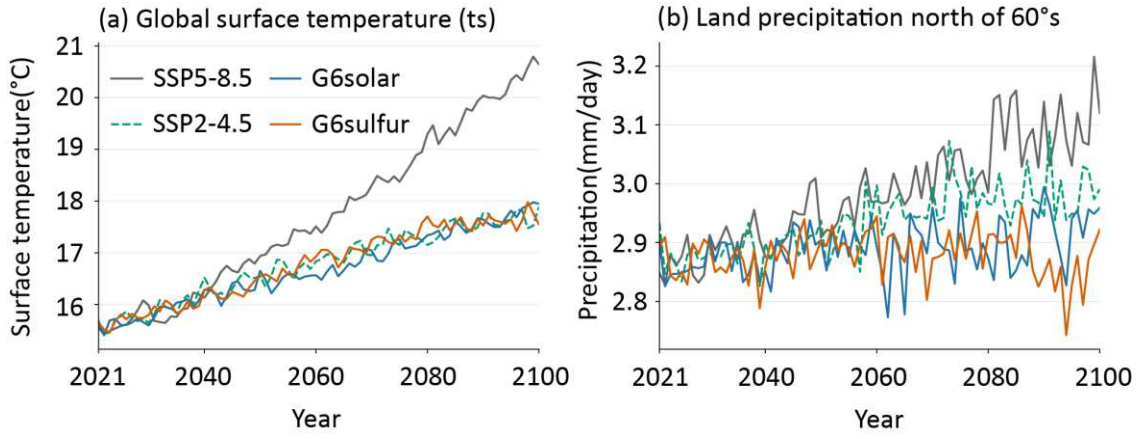


Figure 1: Global mean surface temperature and land mean precipitation during 2021-2100. Annual area-weighted means of (a) surface temperature over the globe and (b) precipitation over land north of 60°S from IPSL-CM6A-LR under SSP5-8.5, SSP2-4.5, G6solar, and G6sulfur.

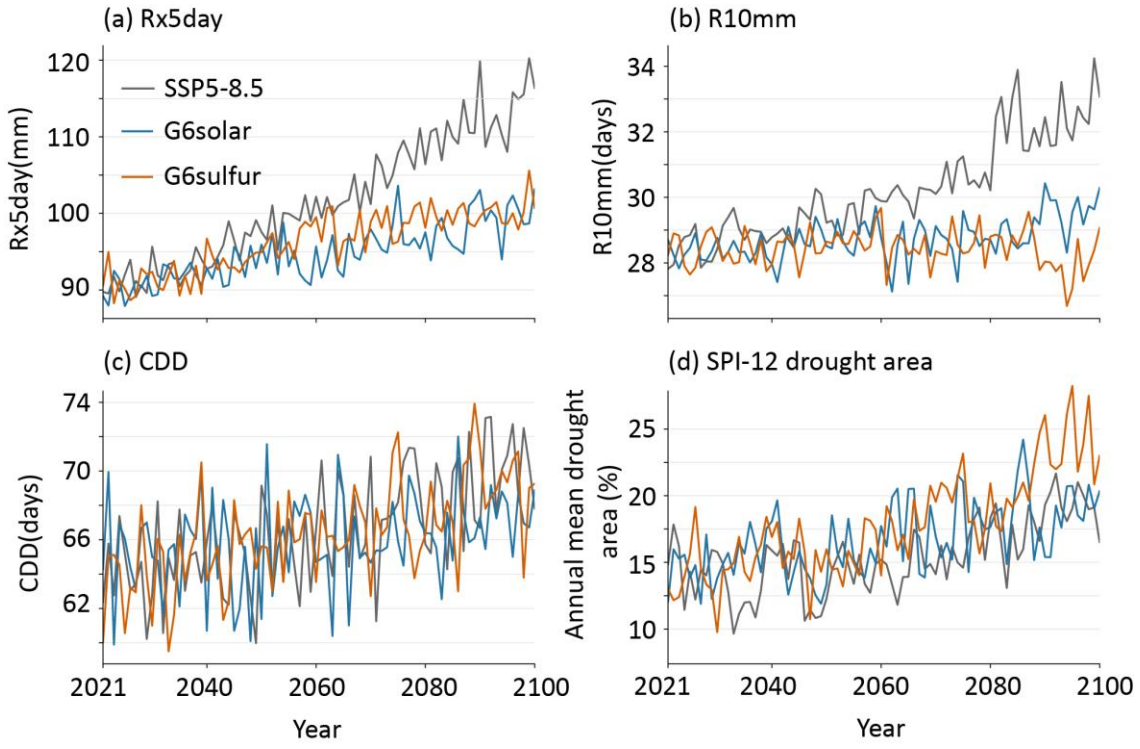


Figure 2: Temporal evolution of land mean precipitation indices and drought area during 2021–2100. Panels show area-weighted means of (a) Rx5day, (b) R10mm, (c) CDD, and (d) the annual mean fraction of land experiencing SPI-12 drought under SSP5-8.5, G6solar, and G6sulfur. Drought months are defined as SPI-12 ≤ -1 using a fixed 1985–2014 reference distribution. Panel (d) averages monthly drought-area fractions within each year, equivalent to the area-weighted annual drought-month fraction over the fixed valid domain.

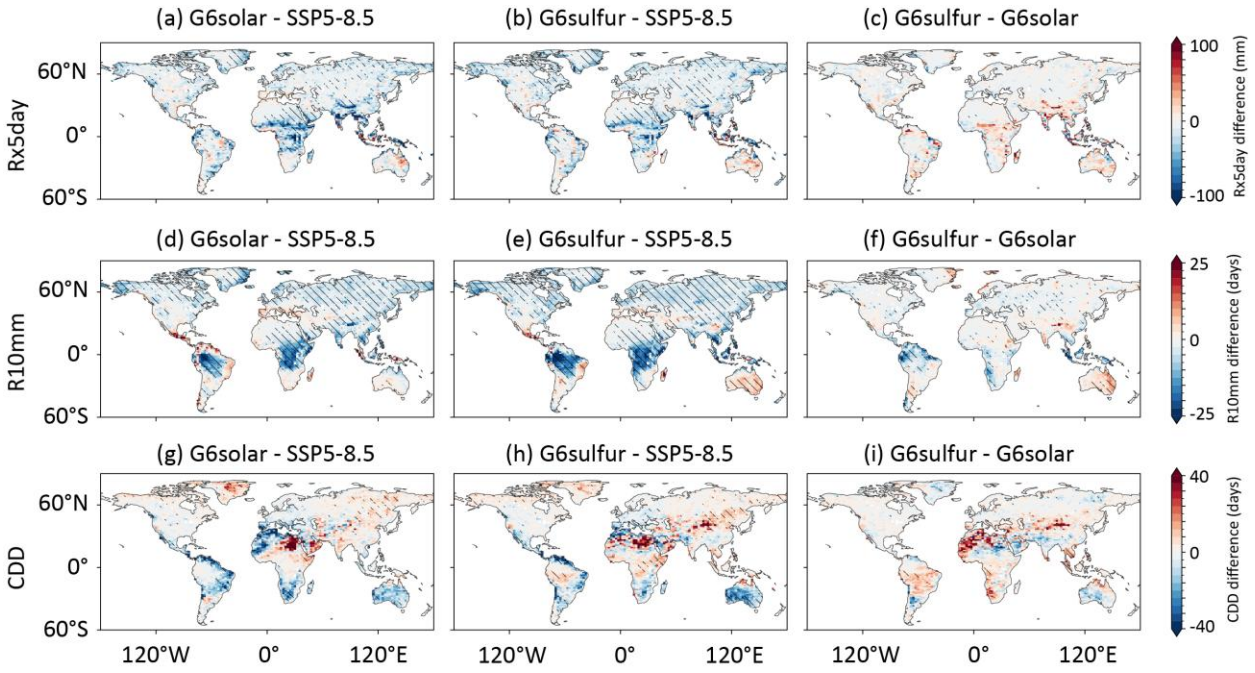


Figure 3: Spatial differences in precipitation indices during 2081–2100. Rows show Rx5day (a-c), R10mm (d-f), and CDD (g-i). Columns show G6solar-SSP5-8.5, G6sulfur-SSP5-8.5, and G6sulfur-G6solar, respectively. Blue and red indicate decreases and increases. Hatching marks grid cells passing two-sided tests, with false discovery rate correction at q=0.05 applied separately for each index and contrast.

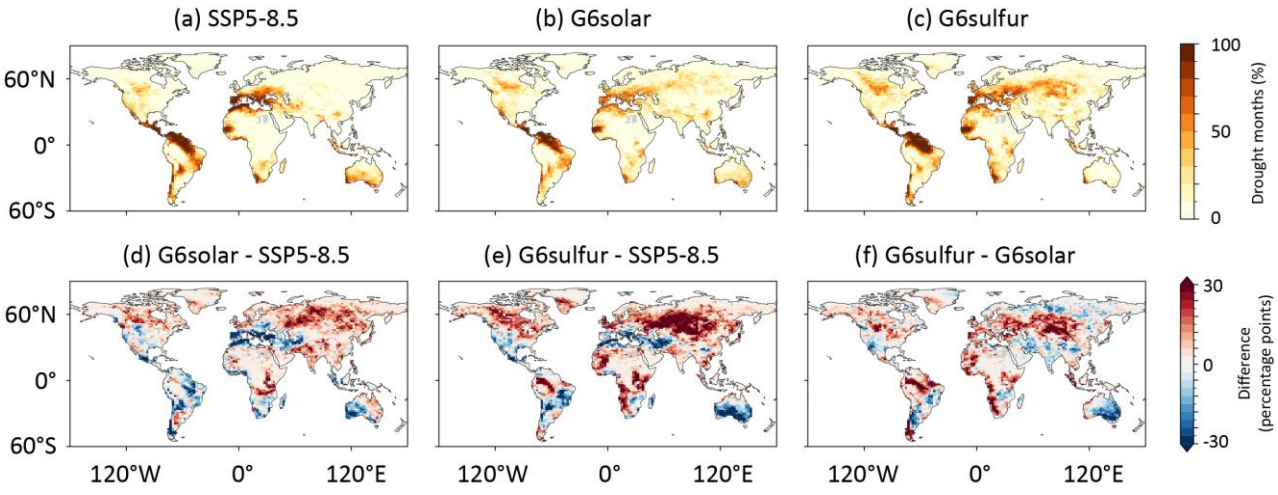


Figure 4: Spatial patterns of SPI-12 drought-month fraction and experiment differences during 2081–2100. Panels (a–c) show the percentage of months with SPI-12 ≤ −1 under SSP5-8.5, G6solar, and G6sulfur; panels (d–f) show G6solar − SSP5-8.5, G6sulfur − SSP5-8.5, and

G6sulfur − G6solar, respectively. SPI-12 uses a fixed 1985–2014 reference distribution, and differences are expressed in percentage points.Hatching marks grid cells passing two-sided tests, with false discovery rate correction at q=0.05 applied separately for each index and contrast.

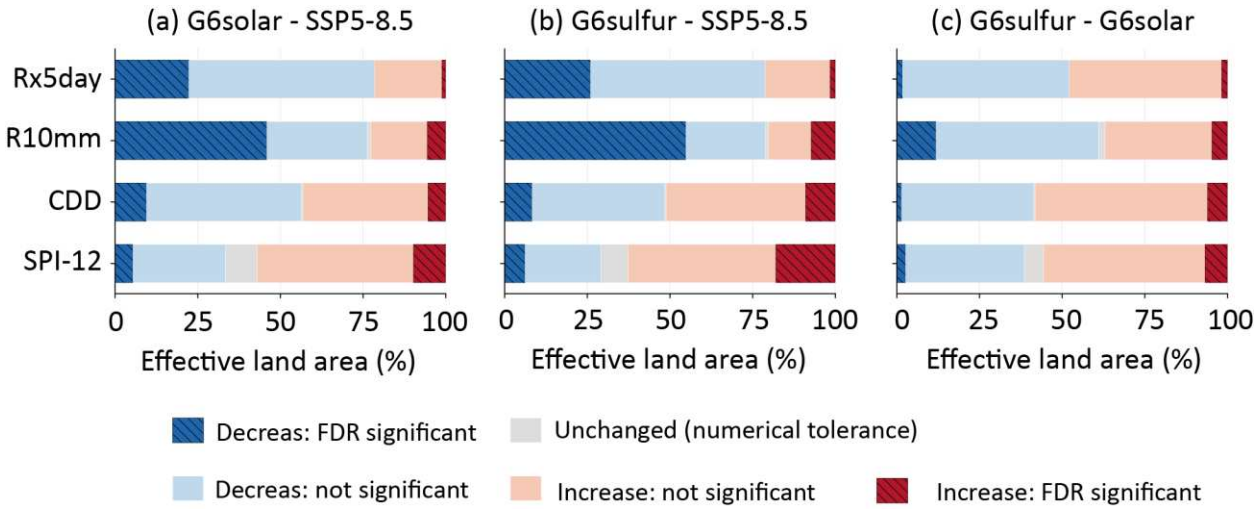


Figure 5: Land area fractions showing increases and decreases during 2081–2100. Panels show (a) G6solar-SSP5-8.5, (b) G6sulfur-SSP5-8.5, and (c) G6sulfur-G6solar for Rx5day, R10mm, CDD, and SPI-12 drought-month. Fractions are weighted by grid-cell area and normalized by the valid land area for each metric.

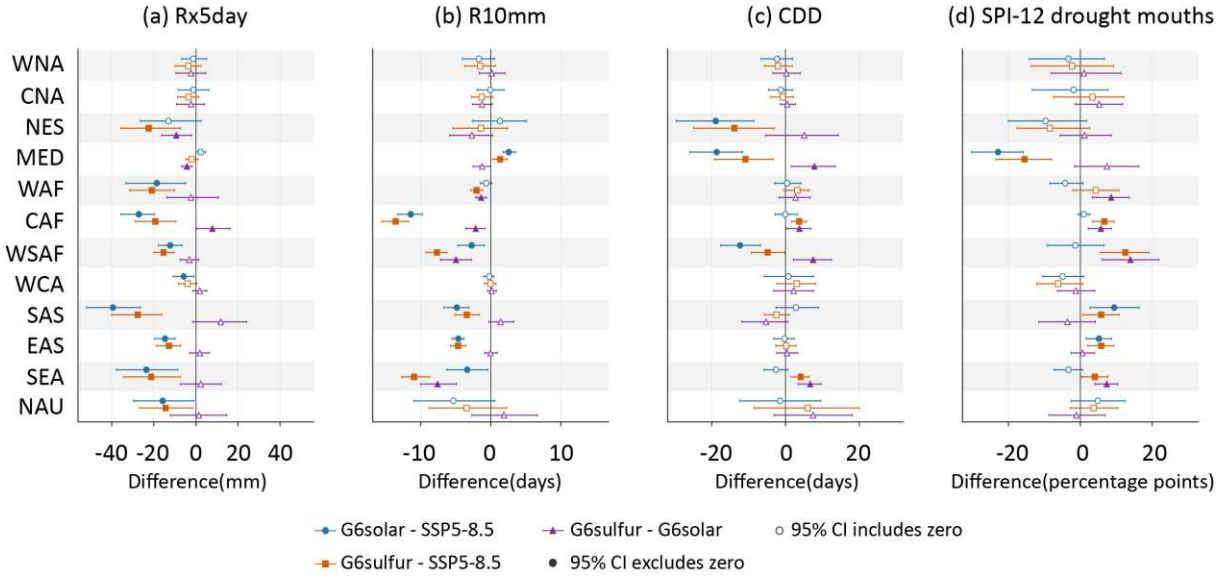


Figure 6: Regional mean differences in precipitation indices and SPI-12 drought-month fraction during 2081–2100. Panels show (a) Rx5day, (b) R10mm, (c) CDD, and (d) SPI-12 drought-month fraction in selected AR6 land regions. Horizontal bars show 95% intervals from independent five-year circular moving-block bootstrap resampling of annual regional series. Regions are western North America (WNA), central North America (CNA), northeastern South America (NES), the Mediterranean (MED), western Africa (WAF), central Africa (CAF), western southern Africa (WSAF), west central Asia (WCA), South Asia (SAS), East Asia (EAS), Southeast Asia (SEA), and northern Australia (NAU).

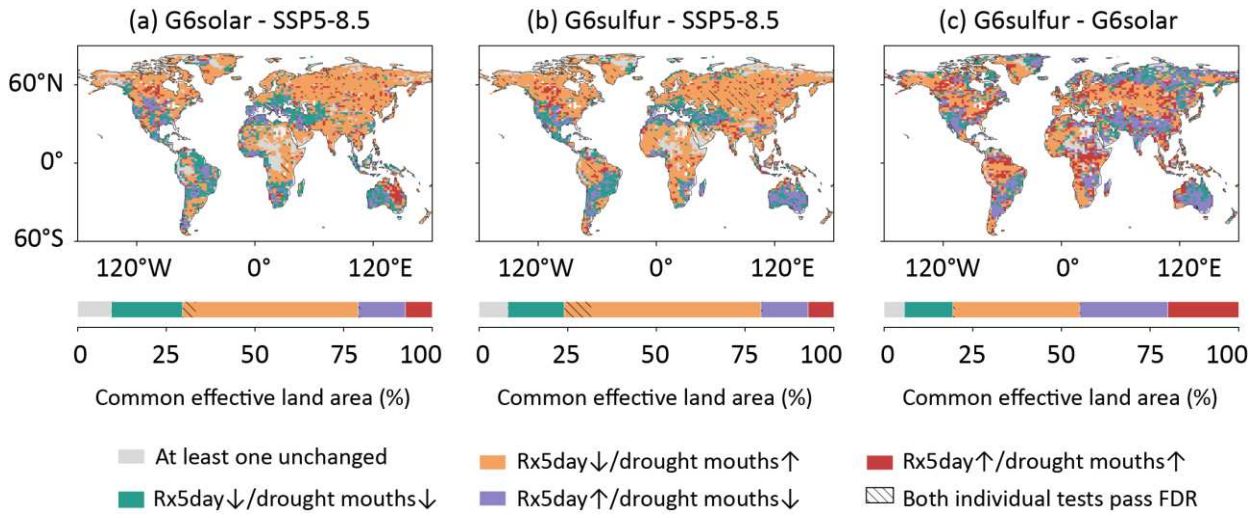


Figure 7: Joint spatial responses of Rx5day and SPI-12 drought-month fraction during 2081–2100. Panels show (a) G6solar − SSP5-8.5, (b) G6sulfur − SSP5-8.5, and (c) G6sulfur − G6solar over land north of 60°S.Hatching marks cells where both indices individually pass their respective FDR-adjusted tests at q = 0.05..

727

728 Table 1: Definitions of the precipitation and drought indices used in this study.

Index	Name	Definition	Expression	Unit	Category
Rx5day	Maximum five-day precipitation	Annual maximum precipitation accumulated over five consecutive days.	$Rx5day_y = max_j({P^{(5)}}_{y,j})$	mm	Intensity
R10mm	Heavy precipitation days	Annual number of days with daily precipitation ≥ 10 mm.	$R10mm_y = \sum_{d \in y} I(P_d \geq 10)$	days	Frequency
CDD	Consecutive dry days	Longest run of days with daily precipitation < 1 mm within a calendar year.	$CDD_y = max_{r \in R_y}(\ell_r)$	days	Duration
SPI-12	12-month standardized precipitation index	Standard normal transformation of the historical cumulative probability of 12-month accumulated precipitation.	$SPI-12_t = \Phi^{-1}[H_m({A^{(12)}}_t)]$	1	Standardized precipitation deficit
SPI-12 drought-month fraction	Annual fraction of drought months	Percentage of months in a year with SPI-12 ≤ −1.	$F_{12,y} = \frac{100}{12}\sum_{m=1}^{12} I(SPI-12_{y,m} \leq -1)$	%	Drought-month occurrence

729

730